High-order boundary conditions for linearized shallow water equations with stratification, dispersion and advection

Vince J. van Joolen[1,‡], Beny Neta[1,*,†] and Dan Givoli[2,§]

[1]*Department of Mathematics, Naval Postgraduate School, 1141 Cunningham Road, Monterey,
CA 93943, U.S.A.*
[2]*Department of Aerospace Engineering, Asher Center for Space Research,
Technion—Israel Institute of Technology, Haifa 32000, Israel*

SUMMARY

The two-dimensional linearized shallow water equations are considered in unbounded domains with density stratification. Wave dispersion and advection effects are also taken into account. The infinite domain is truncated via a rectangular artificial boundary $\mathscr{B}$, and a high-order open boundary condition (OBC) is imposed on $\mathscr{B}$. Then the problem is solved numerically in the finite domain bounded by $\mathscr{B}$. A recently developed boundary scheme is employed, which is based on a reformulation of the sequence of OBCs originally proposed by Higdon. The OBCs can easily be used up to *any* desired order. They are incorporated here in a finite difference scheme. Numerical examples are used to demonstrate the performance and advantages of the computational method, with an emphasis is on the effect of stratification. Published in 2004 by John Wiley & Sons, Ltd.

KEY WORDS: waves; shallow water; stratification; high-order; artificial boundary; open boundary condition; Higdon; Klein–Gordon; finite difference; auxiliary variables

1. INTRODUCTION

Phenomena involving the propagation of waves in very large (or unbounded) domains are applicable to many fields including acoustics, electromagnetics, meteorology, and geophysics. However, it is infeasible to compute numerical solutions for regions of this scope. Therefore, it is necessary to define artificial boundaries that reduce the size of the domain. To accurately model the wave action in the truncated region, one must impose artificial boundary conditions

that allow waves propagating inside the region to pass freely without spurious reflections, which would otherwise pollute the computational domain. Such a boundary condition is known in various names (see, e.g. Reference [1]) and in the context of meteorology mainly as an open boundary condition (OBC).

A strictly mathematical treatment of absorbing boundary conditions for hyperbolic equations was presented by Engquist and Majda [2, 3] based on pseudo-differential operators subsequently expanded to non-local operators to get local well-posed conditions. These methods can be viewed as a generalization of the Sommerfield radiation condition and the characteristic approach. A second alternative approach is the use of sponge or damping layers to damp out disturbances prior to their reaching the artificial boundary. A variation of this process is to construct a layer where the outgoing waves will slow down rather than decay. Hence, the waves will not reflect back into the limited-area forecast domain of interest except at very late times (see References [4–6]). The coupled ocean/atmosphere mesoscale prediction system (COAMPS) involves an atmosphere and an ocean model (see Reference [7]). The equations governing each of these models are solved in a finite computational domain. Thus, there is a need to apply appropriate boundary conditions on the remote boundaries. Lateral boundary conditions implemented in COAMPS today are, in order of complexity,

1. fixed conditions,
2. periodic conditions,
3. zero-order radiation conditions, and
4. the Davies Lateral Sponge Layers [5].

While this remote-boundary treatment of Davies [5] is efficient and may be sufficiently accurate in some cases of interest, it is not so robust in that it is not directly associated with the notion of convergence.

A more recent development, which is not in COAMPS, is the use of perfectly matched layers (PML) method introduced by Berenger [8]. This approach can be viewed as an improvement on the original idea of sponge layers since the PML approach allows the solution in the layer to decay for all angles and frequencies. To be more precise, one surrounds the computational domain with a finite-thickness layer of specially designed model medium which attenuates all the waves that propagate from inside the domain. The parameters of the layer are chosen such that the wave either never reaches the external boundary, or, if it reaches it, it does reflect back and by the time it reaches the interface between the absorbing (sponge) layer and interior computational domain its amplitude is so small that it will not contaminate the solution. The interface between computational domain and the layer should cause minimal or zero reflection, the latter case being called the PML (see also References [9–17]).

In meteorology, one distinguishes between a global model (GM), in which the atmospheric equations are solved over the entire spherical surface of the globe, and a limited-area model (LAM), in which the solution is sought in a relatively small region Ω bounded by artificial boundaries. One very important question in computational meteorology concerns the way in which the information obtained from the GM is incorporated in the LAM. One can use a 'relaxation layer' for gradual transition from the LAM solution to the GM solution. One such scheme has been proposed in 1976 by Davies [5], and is still used today in the Navy code COAMPS [7] when using real data simulations. The global information is taken from the code NOGAPS, Navy Operational Global Atmospheric Prediction System. One can also

use Perkey–Kreitzberg [4] boundary conditions. Our paper is concerned only with the non-reflecting (absorbing) part of the boundary condition, and the blending of global data should be done on top of this using some 'blending scheme.'

In general, it is not possible to construct a boundary condition that will be perfect in all respects, but during the last 25 years research has been conducted to develop OBCs that after discretization lead to stable, accurate, efficient and easily implemented schemes [1, 18–20]. Investigations in the late 1970s to early 1980s produced a number of low-order local OBCs, e.g. the Engquist–Majda [3] and Bayliss–Turkel [21] boundary conditions. The exact non-local Dirichlet-to-Neumann (DtN) OBC [22, 23] and the perfectly matched layer (special damping regions) [8] boundary conditions were developed in the late 1980s and early 1990s.

High-order OBCs were theoretically available since the 1980s but were regarded as impractical beyond 2nd or 3rd order. Only since the mid 1990s have practical higher-order schemes been developed. Collino [24] proposed such a scheme for two-dimensional time-dependent wave in a rectangular domain. Grote and Keller [25] extended the domain to three dimensions in a scheme based on spherical harmonic transformations. They extended their work to include elastic waves [26]. These finding were independently published by Sofronov [27] in Russian literature. Hagstrom and Hariharan [28] constructed high-order OBCs for two- and three-dimensional domains based on the analytic series representation for the outgoing solutions of these equations. Guddati and Tassoulas [29] devised a high-order OBC scheme for time-dependent waves in a 2-dimensional wave guide using rational approximation and recursive continued fractions. Givoli [30] derived high-order OBCs for a general class of wave problems leading to a symmetric finite element formulation. These early investigations utilized either time-harmonic waves or non-dispersive time-dependent waves in a homogeneous medium.

Wave dispersion, however, is an ever present phenomenon in meteorology. In the late 1980s and early1990s, Higdon developed OBCs for non-dispersive waves [31–34], but later showed that his schemes could be applied to the dispersive (Klein–Gordon) wave equation [35]. Higdon's work involves low-order formulation of his scheme. Givoli and Neta [36–38] presented an algorithm for implementing the Higdon OBC to any order using high-order FD discretization. They further developed methods to rewrite the Higdon OBC without using high order derivatives and to generate Higdon parameters that maximize the non-reflection property of the OBC in a dispersive wave environment. Only homogeneous media and wave-guide geometries were considered in these papers.

In the present work, we develop high-order Higdon OBC schemes for use with linearized shallow water equations (SWEs) in Cartesian co-ordinates with wave dispersion. We further enhance the SWE model to include the effects of stratification and advection. We apply the Higdon OBCs to all sides of a rectangular domain to restrict an infinite plane. We use finite-difference schemes to numerically solve the problems. We then employ discrete forms of the Higdon OBC, based on the work of Givoli and Neta [37], on the artificial boundary. We report the results of several numerical examples to validate the use of the Higdon OBC as an effective means of restricting a very large domain.

In the next section, we describe the stratified linear model. In Section 3, we describe the high order Higdon OBC. The discretization of the advective and stratified model is discussed in Section 4. Section 5 presents some of the numerical experiments performed with the linear SWEs with and without stratification. These experiments demonstrate the effectiveness of the method.

2. AN N-LAYER STRATIFIED DISPERSIVE WAVE MODEL

The SWEs, see e.g. Reference [39], are

$$
\frac{\partial u}{\partial t} + u\frac{\partial u}{\partial x} + v\frac{\partial u}{\partial y} - fv = -g\frac{\partial \eta}{\partial x}
$$
$$
\frac{\partial v}{\partial t} + u\frac{\partial v}{\partial x} + v\frac{\partial v}{\partial y} + fu = -g\frac{\partial \eta}{\partial y}
$$
(1)

$$
\frac{\partial \eta}{\partial t} + \left(\frac{\partial(\eta u)}{\partial x} + \frac{\partial(\eta v)}{\partial y}\right) = 0
$$
(2)

Here t is time, $u(x,y,t)$ and $v(x,y,t)$ are the unknown velocities in the x and y directions, $\eta(x,y,t)$ is the unknown water elevation, f is the Coriolis parameter, and g is the gravity acceleration. To linearize we assume that the u,v, and η are dominated by constant terms U, V, and H_0, such that

$$
u = U + u^*, \quad v = V + v^*, \quad \eta = H_0 + \eta^*
$$
(3)

The linearized shallow water model is then

$$
\frac{\partial u^*}{\partial t} + U\frac{\partial u^*}{\partial x} + V\frac{\partial u^*}{\partial y} - f(V + v^*) = -g\frac{\partial \eta}{\partial x}
$$
$$
\frac{\partial v^*}{\partial t} + U\frac{\partial v^*}{\partial x} + V\frac{\partial v^*}{\partial y} + f(U + u^*) = -g\frac{\partial \eta}{\partial y}
$$
$$
\frac{\partial \eta}{\partial t} + U\frac{\partial \eta}{\partial x} + V\frac{\partial \eta}{\partial y} + H_0\left(\frac{\partial u^*}{\partial x} + \frac{\partial v^*}{\partial y}\right) = 0
$$
(4)

van Joolen [39] has shown that system (4) can be written as

$$
\frac{D^2\eta}{Dt^2} - C_0^2\nabla^2\eta + f^2\eta = 0
$$
(5)

where $C_0 = \sqrt{gH_0}$ and the operator $\frac{D}{Dt}$ is given by

$$
\frac{D}{Dt} = \frac{\partial}{\partial t} + U\frac{\partial}{\partial x} + V\frac{\partial}{\partial y}
$$
(6)

Equation (5) is the Klein–Gordon form of the linearized SWEs with non-zero advection. It can also be written as

$$
\frac{\partial^2\eta}{\partial t^2} + (U^2 - C_0^2)\frac{\partial^2\eta}{\partial x^2} + (V^2 - C_0^2)\frac{\partial^2\eta}{\partial y^2}
$$
$$
+ 2U\frac{\partial^2\eta}{\partial x\partial t} + 2V\frac{\partial^2\eta}{\partial y\partial t} + 2UV\frac{\partial^2\eta}{\partial x\partial y} + f^2\eta = 0
$$
(7)

This is an expanded Klein–Gordon equivalent for the linearized SWEs with non-zero advection terms U and V. It applies to a single-layer model, but will be extended to the N-layer stratified model. In case the mean flow $U = V = 0$, we have

$$\frac{\partial u^*}{\partial t} - fv^* = -g\,\frac{\partial \eta}{\partial x}$$

$$\frac{\partial v^*}{\partial t} + fu^* = -g\,\frac{\partial \eta}{\partial y} \tag{8}$$

$$\frac{\partial \eta}{\partial t} + H_0\left(\frac{\partial u^*}{\partial x} + \frac{\partial v^*}{\partial y}\right) = 0$$

These equations can be combined into one equation for η called the Klein–Gordon equation

$$\frac{\partial^2 \eta}{\partial t^2} - C_0^2 \nabla^2 \eta + f^2 \eta = 0 \tag{9}$$

The non-linear SWEs were derived in part from the continuity equation for *homogeneous*, incompressible fluids

$$\frac{\partial u}{\partial x} + \frac{\partial v}{\partial y} + \frac{\partial w}{\partial z} = 0$$

where w is the velocity in the z direction. This critical step in the derivation is no longer possible when we assume that the density ρ is dependent on z.

We now develop a layered shallow water approximation where ρ is constant in each layer (Figure 1). Here it is assumed that the fluid is still incompressible and that the density ρ_i is constant in each layer L_i, but varies in the different layers. In order for this stratification scheme to be stable, ρ_i first be monotonically increasing downward [41]. Additionally we assume that there is no fluid mixing between layers.

Referring to the N-layer shallow water model, the pressure p_i, at any point in L_i is determined from hydrostatic principles

$$p_i = P_0 + g\left(\sum_{m=1}^{i-1} \rho_m h_m + \rho_i \sum_{m=i}^{N}(h_m - z)\right) \tag{10}$$

where P_0 is a constant ambient pressure at the surface, h_i is the water elevation in L_i, and N is the total number of layers in the model. In (10), the first summation term is the contribution to p_i from the layers above L_i. The second summation term is the contribution to p_i from the liquid column in L_i. Thus the horizontal momentum equations in L_i

$$\frac{\partial u_i}{\partial t} + u_i\,\frac{\partial u_i}{\partial x} + v_i\,\frac{\partial u_i}{\partial y} - fv_i = -g\left(\sum_{m=i}^{i-1} \frac{\rho_m}{\rho_i}\,\frac{\partial h_m}{\partial x} + \sum_{m=1}^{N} \frac{\partial h_m}{\partial x}\right)$$

$$\frac{\partial v_i}{\partial t} + u_i\,\frac{\partial v_i}{\partial x} + v_i\,\frac{\partial v_i}{\partial y} + fu_i = -g\left(\sum_{m=1}^{i-1} \frac{\rho_m}{\rho_i}\,\frac{\partial h_m}{\partial y} + \sum_{m=i}^{N} \frac{\partial h_m}{\partial y}\right) \tag{11}$$

where u_i, and v_i are the x-, and y-components of velocity in L_i. It can he shown that

$$\frac{\partial}{\partial t}\,h_i + \frac{\partial}{\partial x}(u_i h_i) + \frac{\partial}{\partial y}(v_i h_i) = 0 \tag{12}$$
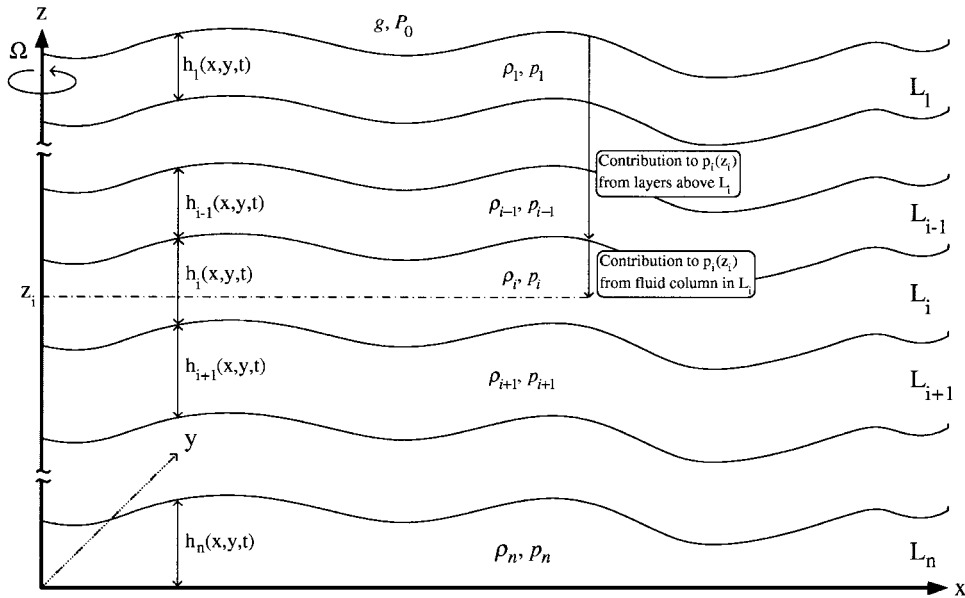
Figure 1. N-Layer shallow water model.

Equation (12) is the vertical momentum equation for L_i. Together with (11) this completes the description of the fluid motion inside of the ith-layer L_i.

To linearize the equations we assume that the u_i, v_i, and h_i are dominated by constant terms U_i, V_i and Θ_i. Superimposed on these are small variations u_i^*, v_i^*, and η_i, i.e.

$$u_i = U_i + u_i^*, \quad v_i = V_i + v_i^* \text{ and } h_i = \Theta_i + \eta_i \tag{13}$$

Substituting these in (11) and (12) and neglecting non-linear terms yields

$$\frac{\partial u_i^*}{\partial t} + U_i \frac{\partial u_i^*}{\partial x} + V_i \frac{\partial u_i^*}{\partial y} - f(V_i + v_i^*) = -g \left(\sum_{m=1}^{i-1} \frac{\rho_m}{\rho_i} \frac{\partial \eta_m}{\partial x} + \sum_{m=i}^{N} \frac{\partial \eta_m}{\partial x} \right)$$

$$\frac{\partial v_i^*}{\partial t} + U_i \frac{\partial v_i^*}{\partial x} + V_i \frac{\partial v_i^*}{\partial y} + f(U_i + u_i^*) = -g \left(\sum_{m=1}^{i-1} \frac{\rho_m}{\rho_i} \frac{\partial \eta_m}{\partial y} + \sum_{m=i}^{N} \frac{\partial \eta_m}{\partial y} \right) \tag{14}$$

$$\frac{\partial \eta_i}{\partial t} + U_i \frac{\partial \eta_i}{\partial x} + V_i \frac{\partial \eta_i}{\partial y} + \Theta i \left(\frac{\partial u_i^*}{\partial x} + \frac{\partial v_i^*}{\partial y} \right) = 0$$

The system of Klein–Gordon equations in this case is

$$\frac{\partial^2 \eta_i}{\partial t^2} + U_i^2 \frac{\partial^2 \eta_i}{\partial x^2} - C_{0_i}^2 \frac{\partial^2}{\partial x^2} \left(\sum_{m=1}^{i-1} \frac{\rho_m}{\rho_i} \eta_m + \sum_{m=i}^{N} \eta_m \right)$$

$$+V_i^2 \frac{\partial^2 \eta_i}{\partial y^2} - C_{0_i}^2 \frac{\partial^2}{\partial y^2} \left(\sum_{m=1}^{i-1} \frac{\rho_m}{\rho_i} \eta_m + \sum_{m=i}^{N} \eta_m \right)$$

$$+2U_i \frac{\partial^2 \eta_i}{\partial x \partial t} + 2V_i \frac{\partial^2 \eta_i}{\partial y \partial t} + 2U_i V_i \frac{\partial^2 \eta_i}{\partial x \partial y} + f^2 \eta_i = 0 \tag{15}$$

In case $U = V = 0$, the above system is reduced to

$$\frac{\partial^2 \eta_i}{\partial t^2} - g\Theta_i \nabla^2 \left(\sum_{m=1}^{i-1} \frac{\rho_m}{\rho_i} \eta_m + \sum_{m=i}^{N} \eta_m \right) + f^2 \eta_i = 0 \tag{16}$$

3. HIGDON-LIKE OBCS

The Higdon condition H_J is given by

$$H_J : \left[\prod_{j=1}^{J} \left(\frac{\partial}{\partial t} + C_j \frac{\partial}{\partial v} \right) \right] \eta = 0 \quad \text{on } \mathscr{B} \tag{17}$$

and is a product of J operators of the form $(\partial/\partial t) + C_j \partial/\partial v$. Higdon showed that the reflection coefficient is given by

$$R = \prod_{j=1}^{J} \left| \frac{C_j - C_x}{C_j + C_x} \right| \tag{18}$$

Since the terms in the product are all less than unity, the reflection coefficient becomes smaller with increasing J no matter what choice of C_j is used. To fix ideas, in this section we consider the east boundary Γ_E where $\partial/\partial v = \partial/\partial x$. The ideas are easily carried over to the three other boundaries as well. We consider the following FD approximations:

$$\frac{\partial}{\partial t} \simeq \frac{I - S_t^-}{\Delta t}, \quad \frac{\partial}{\partial x} \simeq \frac{1 - S_x^-}{\Delta x} \tag{19}$$

In (19), Δt and Δx are, respectively, the time-step size and grid spacing in the x direction, I is the identity operator, and S_t^- and S_x^- are shift operators defined by

$$S_t^- \eta_{pq}^n = \eta_{pq}^{n-1}, \quad S_x^- \eta_{pq}^n = \eta_{p-1,q}^n \tag{20}$$

Note that on the west boundary we will use forward difference operators, so that, only interior points are involved. Here and elsewhere, η_{pq}^n is the FD approximation of $\eta(x, y, t)$ at grid point (x_p, y_q) and at time t_n. We use (19) in (17) to obtain

$$\left[\prod_{j=1}^{J} \left(\frac{I - S_t^-}{\Delta t} + C_j \frac{I - S_x^-}{\Delta x} \right) \right] \eta_{Eq}^n = 0 \tag{21}$$

Here, the index E correspond to a grid point on the boundary Γ_E. Higdon has solved this difference equation (and also a slightly more involved equation that is based on time- and space-averaging approximations for $\partial/\partial x$ and $\partial/\partial t$ for $J \leqslant 3$ to obtain an explicit formula

for η_{Eq}^n. This formula is used to find the current values on the boundary Γ_E *after* the solution in the interior points and on the other boundaries has been updated. The formula for $J = 2$ is found in Reference [42], and the one for $J = 3$ appears in the appendix of Higdon [34]. The algebraic complexity of these formulas increases rapidly with the order J. Now, we show how to implement the Higdon OBCs *to any order* using a simple algorithm. To this end, we first multiply (21) by Δt and rearrange to obtain

$$Z \equiv \left[\prod_{j=1}^{J} (a_j I + d_j S_t^- + e_j S_x^-) \right] \eta_{Eq}^n = 0 \tag{22}$$

where

$$a_j = 1 - e_j \tag{23}$$

$$d_j = -1 \tag{24}$$

$$e_j = -\frac{C_j \Delta t}{\Delta x} \tag{25}$$

The coefficient d_j actually does not depend on j, but we keep this notation to allow easy extensions to the scheme. The coefficient e_j have opposite sign on the west boundary, since we have to have forward shift operator in x, i.e. S_x^+. Now, Z in (22) can be written as a sum of 3^J terms, each one is an operator acting on η_{Eq}^n, namely

$$Z \equiv \sum_{m=0}^{3^J - 1} A_m P_m \eta_{Eq}^n = 0 \tag{26}$$

Here A_m is a coefficient depending on the a_j, d_j and e_j, and P_m is an operator involving products of I, S_t^- and S_x^-. If the interior scheme is explicit (otherwise, see later), all the terms in the sum in (26) are computable at the current time step n, except the one which involves only the identity operator and no shift operators. If we let this term correspond to $m = 0$, then $P_0 = I$ and

$$A_0 = \prod_{j=1}^{J} a_j \tag{27}$$

Thus we get from (26)

$$Z \equiv A_0 \eta_{Eq}^n + Z^* = 0 \tag{28}$$

where

$$Z^* = \sum_{m=1}^{3^J - 1} A_m P_m \eta_{Eq}^n \tag{29}$$

From (28) we get

$$\eta_{Eq}^n = - Z^*/A_0 \tag{30}$$

which is the desired value of η on the boundary Γ_E.

The problem now reduces to calculating Z^* given by (29). We do this using the algorithm proposed by Givoli and Neta [37]. For completeness, we summarize this algorithm in Box 1. The basic idea is to calculate the coefficients A_m and the operator actions $P_m \eta_{Eq}^n$ term by term. This is done systematically by transforming the integer counter m to a number in base 3 with J digits. The A_m and P_m are not simple functions of the decimal representation of the number m, but they *are* simple functions of the digits of the base-3 representation of m.

Note that we need to store $\eta_{iq}^{\hat{n}}$ values for $\hat{i} = E, E-1, \ldots, E-J$ and $\hat{n} = n, n-1, \ldots, n-J$. In other words, we have to store the history of the values of η for a layer of thickness $J+1$ points near the boundary Γ_E and for $J+1$ time levels (including the current one). If there are N_y grid points in the y direction, then the amount of storage needed in a simple storage scheme is $(J+1)^2 N_y$. However, one can save in storage by exploiting the fact that not all values $\eta_{iq}^{\hat{n}}$ are needed, but only those for which $(E-\hat{i}) + (n-\hat{n}) \leqslant J$. This is clear from (17)

- Start with $Z^* = 0$. Calculate $A_0 = \prod_{j=1}^J a_j$.
- Loop over the integers $m = 1, \ldots, 3^J - 1$.
  - For a given m, transform m into a number r in base 3, consisting of the digits 0,1 and 2 only. The length of r will be at most J digits. Store the J digits of r in the vector $D_r(j)$, $j = 1, \ldots, J$.
    Example
    Suppose that $J = 6$ and $m = 227$. Since 227 in base 3 is $r = 22102$, we will get $D_r = \{0\ 2\ 2\ 1\ 0\ 2\}$.
  - Use D_r to calculate the coefficient A_m. To this end, start with $A_m = 1$, loop over $j = 1, \ldots, J$, and for each j multiply A_m by the factor a_j (if $D_r(j) = 0$) or d_j (if $D_r(j) = 1$) or e_j (if $D_r(j) = 2$).
    Example
    For $J = 6$ and $m = 227$, we have received the vector D_r above. Then $A_{227} = a_1 e_2 e_3 d_4 a_5 e_6$.
  - Use D_r to calculate the operator action $P_m \eta_{Eq}^n$. To this end, start with $\hat{n} = n$ and $\hat{i} = E$, loop over $j = 1, \ldots, J$, and for each j subtract 1 from $\hat{n}$ (if $D_r(j) = 1$) or subtract 1 from $\hat{i}$ (if $D_r(j) = 2$) or do nothing (if $D_r(j) = 0$). After the loop ends we have $P_m \eta_{Eq}^n = \eta_{\hat{i}q}^{\hat{n}}$.
    Example
    For the case $J = 6$ and $m = 227$ considered above, we get $\hat{n} = n - 1$ (because the digit '1' appears only once in D_r), and $\hat{i} = E - 3$ (because the digit '2' appears three times in D_r). Hence $P_{227} \eta_{Eq}^n = \eta_{E-3,q}^{n-1}$.
  - Update: $Z^* \leftarrow Z^* + A_m \eta_{\hat{i}q}^{\hat{n}}$.
- Next m.
- $\eta_{Eq}^n = -Z^*/A_0$.

Box 1. Algorithm for implementing the Higdon OBC of order J on the discrete level (first formulation).

Table I. CPU time (s) as a function of J.

J	Time
1	0.01
2	0.01
1	0.01
4	0.05
5	0.15
6	0.51
7	1.74
8	8.14
9	62.68

and also from (22). For example, the solution at time t_{n-J} should be stored only for points on the boundary Γ_E itself.

This formulation of the Higdon OBCs requires penetration into the domain (because of the high normal derivative) and also requires time-history. Thus the storage requirement can be high. Also, in order to work properly the method requires a 'buffer zone' of zero initial conditions, of width J. In addition it is not easy to extend the algorithm to FE formulations and to unstructured meshes. On the other hand, by construction it is stable at the corners.

If the interior scheme is implicit, as is the case when advection is present, we have to exclude from Z^* all terms containing only powers of S_x^-. There are

$$\sum_{k=1}^{J} \binom{J}{k}$$

terms. These terms have index m whose base-3 representation contains only the digits 0 and 2, see Box 1. Now Z^* can be computed based on the previous algorithm. We compute A_m for the terms excluded from Z^* (i.e. for m whose base-3 representation contains only the digits 0 and 2) and create an equation relating boundary values to interior values at time n. This equation will be part of the system in the next section.

An alternative formulation, which eliminates all derivatives in the Higdon condition beyond the second-order ones via the use of *auxiliary variables*, is given in the appendix. This alternative formulation does not require penetration into the domain and the keeping of time-history. It also does not require a 'buffer zone' of zero initial conditions. On the other hand it is potentially less stable (not every combination of C_j in every order gives stability) and it may require special attention at the corners. However, we remark that all (but one) the numerical results presented in Section 5 were obtained by the high-derivative discrete formulation described above. One numerical result using auxiliary variable formulation but no advection is presented in order to demonstrate very high order ($J = 20$) OBCs.

In Table I, we give the overhead CPU time in seconds (using PC/AT with 130 Mb RAM) required as a function of the order J of the boundary conditions. It can be seen that up to $J = 5$, the overhead is negligible.

4. DISCRETIZING THE LINEARIZED SWE N-LAYER STRATIFIED MODEL WITH CONSTANT NON-ZERO ADVECTION TERMS

We have used the central-difference approximations

$$A\eta_{i,pq}^n + D_i\eta_{i,p+1,q}^n - D_i\eta_{i,p-1,q}^n + E_i\eta_{i,p,q+1}^n - E_i\eta_{i,p,q-1}^n$$

$$= (2A + 2B_i + 2C_i - f^2)\eta_{i,pq}^{n-1} - A\eta_{i,pq}^{n-2} - B_i(\eta_{i,p+1,q}^{n-1} + \eta_{i,p-1,q}^{n-1})$$

$$- C_i(\eta_{i,p,q+1}^{n-1} + \eta_{i,p,q-1}^{n-1}) + D_i(\eta_{i,p+1,q}^{n-2} - \eta_{i,p-1,q}^{n-2}) + E_i(\eta_{i,p,q+1}^{n-2} - \eta_{i,p,q-1}^{n-2})$$

$$- F_i(\eta_{i,p+1,q+1}^{n-1} - \eta_{i,p+1,q-1}^{n-1} - \eta_{i,p-1,q+1}^{n-1} + \eta_{i,p-1,q-1}^{n-1})$$

$$+ G_i\left[\sum_{m=1}^{i-1}\frac{\rho_m}{\rho_i}(\eta_{m,p+1,q}^{n-1} - 2\eta_{m,pq}^{n-1} + \eta_{m,p-1,q}^{n-1}) + \sum_{m=i}^{N}(\eta_{m,p+1,q}^{n-1} - 2\eta_{m,pq}^{n-1} + \eta_{m,p-1,q}^{n-1})\right]$$

$$+ H_i\left[\sum_{m=1}^{i-1}\frac{\rho_m}{\rho_i}(\eta_{m,p,q-1}^{n-1} - 2\eta_{m,pq}^{n-1} + \eta_{m,p,q-1}^{n-1}) + \sum_{m=i}^{N}(\eta_{m,p,q+1}^{n-1} - 2\eta_{m,pq}^{n-1} + \eta_{m,p,q-1}^{n-1})\right]$$

$$(31)$$

where

$$A = \frac{1}{\Delta t^2}, \qquad B_i = \left(\frac{U_i}{\Delta x}\right)^2, \quad C_i = \left(\frac{V_i}{\Delta y}\right)^2, \quad D_i = \frac{U_i}{2\Delta x\Delta t}$$

$$E_i = \frac{V_i}{2\Delta y\Delta t}, \quad F_i = \frac{U_i V_i}{2\Delta x\Delta y}, \quad G_i = \left(\frac{C_{0i}}{\Delta x}\right)^2, \quad H_i = \left(\frac{C_{0i}}{\Delta y}\right)^2$$

$$(32)$$

As in the single-layer advection case, (31) must be solved implicitly for each layer L_i. The system of equations is complemented on the boundaries using the discretized Higdon boundary equations as discussed before.

4.1. The Higdon matrix

An image of the coefficient matrix resulting from (31) along with the boundary conditions is presented in Figure 2 where zero elements are black and non-zero elements are white. Here the truncated domain Ω is approximated using 21×21 grid and Higdon OBCs of order $J = 9$ are applied to all four sides. On the top and the bottom of the image we see 10 light diagonal lines. These lines represent the discretization for the y-boundaries Γ_N (top) and Γ_S (bottom). The heavier line along the diagonal is three points thick and is flanked to the left and right by two thinner lines. These result from the discretization of the interior points. Finally, the periodic 'short-spikes' pointing to the left and right were generated by the Higdon OBCs on Γ_E and Γ_W, respectively. Note that there are only 19 **each** of these short horizontal lines. This indicates that the corner points were included in the y-boundaries, otherwise 21 (N_x) of such pairs would be visible.
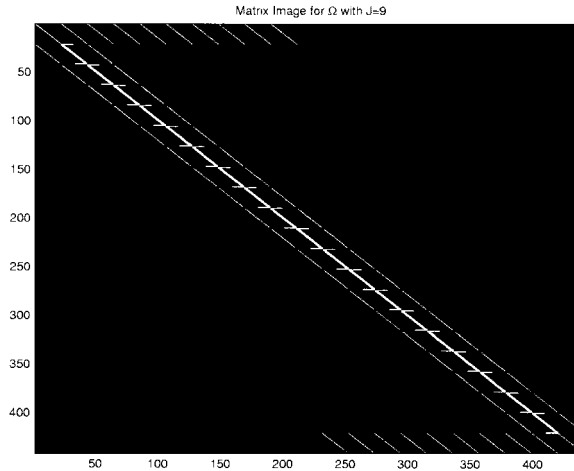
Figure 2. Higdon matrix image for Ω (20×20) with Higdon
NRBCs with order $J = 9$ applied to four sides.

It is evident from the image, that the Higdon matrix required for non-zero advection problem is sparse. The number of non-zero points generated by the domain interior is

$$5(N_x - 2)(N_y - 2) \tag{33}$$

and the number of non-zero points generated by the four Higdon OBCs is

$$(2N_x + 2N_y - 4)(J + 1) \tag{34}$$

Therefore the fraction of non-zero elements in the matrix is

$$\frac{5(N_x - 2)(N_y - 2) + (2N_x + 2N_y - 4)(J + 1)}{N_x^2 N_y^2} \tag{35}$$

In our case where $N_x = N_y = 21$ and $J = 9$, only 1.34% of the matrix elements are non-zeros. lncreasing domain size or number of layers as well as refining the grid would further exacerbate the problem. Clearly sparse matrix procedures are in order.

5. NUMERICAL EXAMPLES

5.1. Two-dimensional single-layer scheme with Higdon OBCs on four sides with non-zero advection

In this example, the truncated domain Ω with Higdon OBCs on four sides is used. The extended domain $\mathscr{D}$ is an infinite plane represented by a 15×15 square with a 60×60 mesh. Ω is located in the centre of $\mathscr{D}$ at $5 \leqslant x, y \leqslant 10$. Higdon boundaries are also imposed on $\mathscr{D}$ for computational purposes. Spurious reflection from these boundaries should not significantly pollute Ω. On both domains $\Delta x = \Delta y = 0.25$ and $\Delta t = 0.0125$. A gravitation parameter of

$g = 10$, dispersion parameter of $f = 0.5$, and a single layer of thickness $\Theta = 0.1$ with density $\rho = 1$ is used. Advection constants of $U = 0.5$ and $V = -0.25$ are utilized.

Physical disturbances in Ω are initiated via two separate events. Event 1 is given by

$$S^{t=0.025} = \begin{cases} 0.0001 \times \text{rand}(-0.5, 0.5) & \text{if } 1.5 \leqslant x, y \leqslant 3.5 \\ 0 & \text{otherwise} \end{cases} \qquad (36)$$

where $S^{t=0.025}(x, y)$ represents a disturbance initiated at $t = 0.025$ and $\text{rand}(-0.5, 0.5)$ is a random number on the interval $[-0.5, 0.5]$. Event 2 is given by

$$S^{t=5} = \begin{cases} 0.000015 \times \text{rand}(-0.25, 0.75) & \text{if } 1.5 \leqslant x \leqslant 2.25 \ \& \ 1.5 \leqslant y \leqslant 3.5 \\ 0 & \text{otherwise} \end{cases} \qquad (37)$$

where $S^{t=5}(x, y)$ represents a disturbance initiated at $t = 5$ and $\text{rand}(-0.25, 0.75)$ is a random number on the interval $[-0.25, 0.75]$. A buffer of at least 5 zero-valued grid points was maintained between the OBC and each event for stability purposes. The events are shifted 5 units in the positive x- and y-directions on $\mathscr{D}$ in order to properly place them in the domain's centre.

Before running an example, consideration was given to the selection of C_j's. Several experiments were conducted with results reported in Plate 1. Initially, a Higdon OBC with order $J = 5$ and $C_j = \{C_0, C_0, C_0, C_0, C_0\}$ where $C_0 = \sqrt{g\Theta} = 1$ was considered. This was compared to a case where the C_j's are corrected for advection. The predominate speed of the gravity wave is C_0. This is affected somewhat the dispersion and wave height. However, with the inclusion of advection, the predominate wave speed with respect to each boundary is affected more significantly. Therefore the C_j's on each boundary are adjusted. These adjustments were made as follows:

$$\begin{aligned} C_j^{\text{east}} &= C_j + U, & C_j^{\text{west}} &= C_j - U \\ C_j^{\text{north}} &= C_j + V, & C_j^{\text{south}} &= C_j - V \end{aligned} \qquad (38)$$

For this example, the adjusted C_j's are

$$C_j^{\text{east}} = \{1.5, 1.5, 1.5, 1.5, 1.5\}, \quad C_j^{\text{north}} = \{0.75, 0.75, 0.75, 0.75, 0.75\}$$

$$C_j^{\text{west}} = \{0.5, 0.5, 0.5, 0.5, 0.5\}, \quad C_j^{\text{south}} = \{1.25, 1.25, 1.25, 1.25, 1.25\}$$

We define the error norm $\|e(t)\|_\Omega$ by the square root of the some of the squares of the pointwise difference between the solution on the truncated domain Ω and the solution on the extended domain. The results of both runs show a significant decrease in $\|e(t)\|_\Omega$ to about 10^{-3} at $t = 10$. This error, however, can be reduced further.

A buffer of J zero-valued grid points was necessary to achieve stability for a Jth-order Higdon OBC. When advection is incorporated into the problem, this buffer zone moves horizontally toward at least one of the boundaries. Therefore the buffer is compressed with respect to the boundary toward which it is moving. In order to maintain stability we must either increase the size of the buffer zone, or reduce the order J. In plot B (top right) of Plate 1 a 5th-order Higdon OBC is compared to a 3rd-order Higdon OBC. In both cases the C_j's

are adjusted for advection. In this example, $\|e(t)\|_\Omega$ is reduced by an order of magnitude to about 10^{-4}.

One further adjustment is possible to reduce $\|e(t)\|_\Omega$. Geometric dispersion is another factor in the boundaries response to an impinging wave. A wave striking normal to the boundary will generally have a wave speed that is approximately C_0. In all other cases, the wave speed is less than C_0. An example was set up for $J = 3$ in which $C_j = \{0.8, 0.9, 1\}$ with the reduced values taking into account the geometric dispersion. Adjusted for advection, the C_j's used for the problem are

$$C_j^{\text{east}} = \{1.3, 1.4, 1.5\}, \quad C_j^{\text{north}} = \{0.55, 0.65, 0.75\}$$

$$C_j^{\text{west}} = \{0.3, 0.4, 0.5\}, \quad C_j^{\text{south}} = \{1.05, 1.15, 1.25\}$$

$$(39)$$

In Plot C (bottom left) of Plate 1 an additional reduction in $\|e(t)\|_\Omega$ is evident. Further analysis is necessary to determine how to best adjust C_j values for geometric dispersion.

The question of the corner points of Ω is again salient in the advection case, because the values for C_j on each boundary are now different. Recall that there are two ways to approximate the boundary values when numerically solving the problem. Both approaches are tested here. In the first run the x-boundaries were computed first (including the corner points) and the y-boundaries computed next (excluding the corner points). In a second experiment the procedure was reversed and corner points were included in the y-boundaries. Plot D (bottom right) of Plate 1 reveals that the solutions are identical. Hence, as concluded earlier, no special handling at the corner points is necessary.

With these results in mind, Higdon OBCs of order $J = 3$ with $C_j = \{0.8, 0.9, 1\}$ are used. With $U = 0.5$ and $V = -0.25$, the adjusted C_j's are those listed in (39). A trial is run for 10 time units. At $t = 1$ (Plate 2), event 1 has been propagating outward in Ω for approximately 1 time unit. The effect of advection is apparent as the propagation of the gravity wave is tending toward the southeast (i.e. in the $< 0.5, -0.25 >$ direction). The leading edge of the wave has passed through the Γ_E, but the error measurement is still very small. At $t = 2$ (Plate 3), event 1 has crossed Γ_S and Γ_E. Later, at $t = 3$ (Plate 4), event 1 has crossed Γ_N and Γ_W. At $t = 5$ (Plate 5), most of event 1 has left Ω. We note some spurious activity on the western boundary.

At $t = 6$ (Plate 6), the waves generated by event 2 are approaching Γ_E and Γ_W. Event 1 has passed through all four boundaries relatively unperturbed. The plot of $\mathscr{D}$ reveals that the wave front continues to tend toward the southern and eastern portion of the extended domain.

At $t = 10$ (Plate 7), the second event has passed through the boundary. The wave propagation pattern continues to 'drift' in the direction of advection as revealed by the upper-right plot of $\mathscr{D}$. Close inspection of the contours reveal spreading where the gravity wave is travelling in the direction of advection and compression where the gravity wave is travelling against the direction of advection. In the latter case, this indicates a steeper wave front. Since the gravity wave is omni-directional, this effect varies throughout the plot. In Ω the noise of spurious reflection is now visible.

This experiment was repeated for two other sets of values for U and V. In the first variation (Plate 8) the magnitude of the advection constants were lowered to $U = 0.4$ and $V = -0.15$. As expected, there is a decreased tendency toward the southeast. Also notable is a reduction in the error measurement.
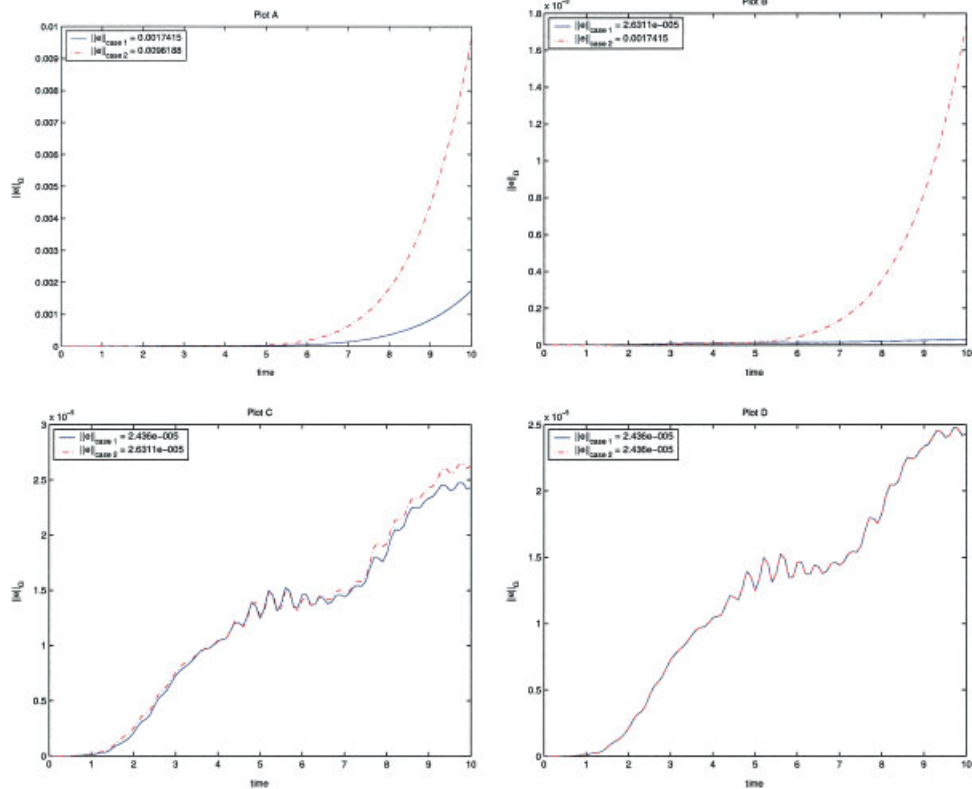
Plate 1. Plot A (top left): $J = 5$ with $C_j = \{1, 1, 1, 1, 1\}$ adjusted for advection compared to $J = 5$ with $C_j = \{1, 1, 1, 1, 1\}$ unadjusted for advection. Plot B (top right): $J = 3$ with $C_j = \{1, 1, 1\}$ compared to $J = 5$ with $C_j = \{1, 1, 1, 1, 1\}$, both cases adjusted for advection. Plot C (bottom left): $J = 3$ with $C_j = \{0.8, 0.9, 1\}$ compared to $J = 3$ with $C_j = \{1, 1, 1\}$, both cases adjusted for advection. Plot D (bottom right): Corner check for $J = 3$ with $C_j = \{0.8, 0.9, 1\}$ adjusted for advection.
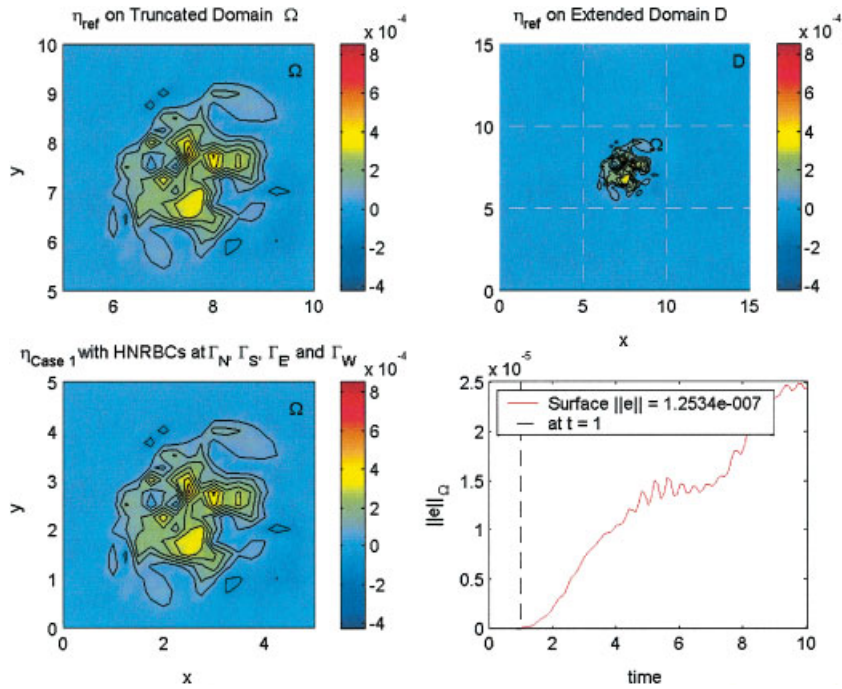
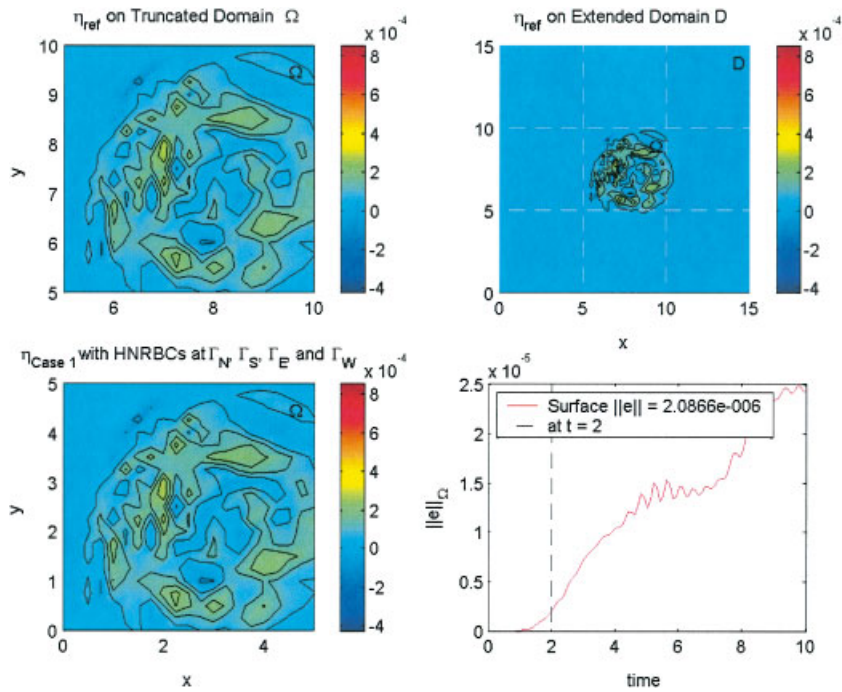Plate 2. Single layer problem, the solution at $t=1$ after the first event has been initiated.

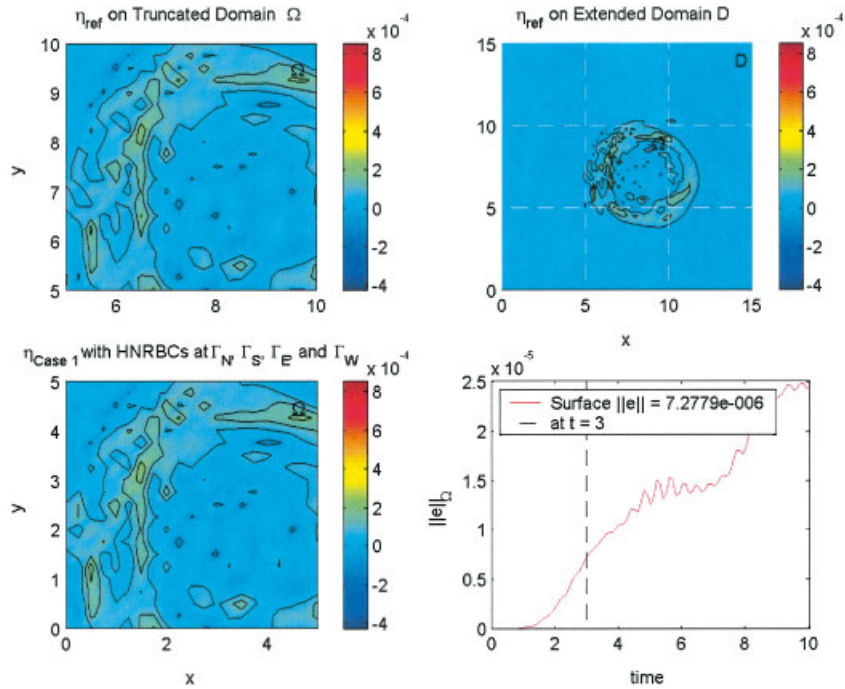Plate 3. Single layer problem, the solution at $t=2$ after the first event crosses Γ_S and Γ_E.

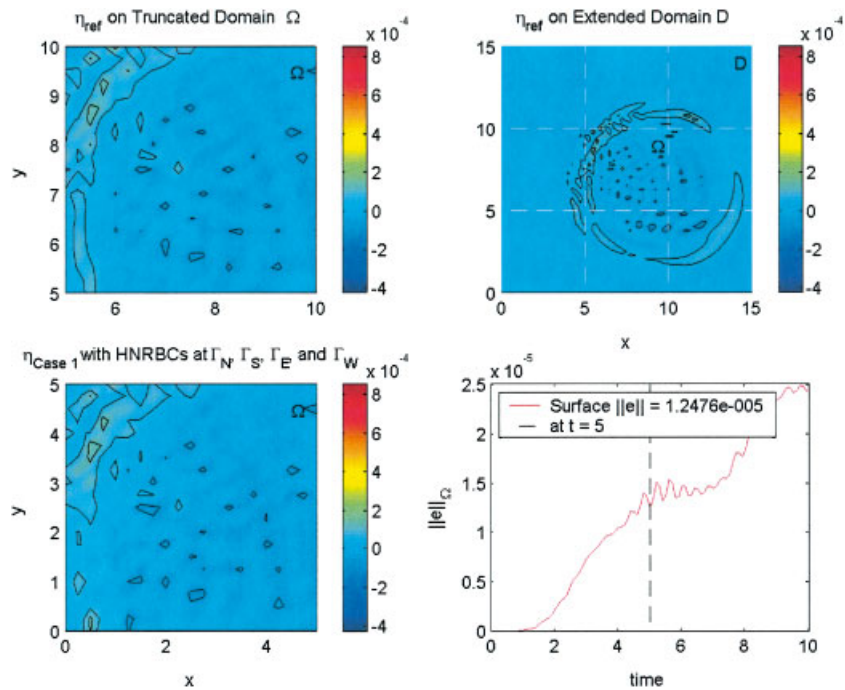Plate 4. Single layer problem, the solution at $t = 3$ after the first event crosses Γ_N and Γ_W.

Plate 5. Single layer problem, the solution at $t = 5$ after the first event leaves Ω with visible spurious reflection at Γ_W.

Published in 2004 by John Wiley & Sons, Ltd.

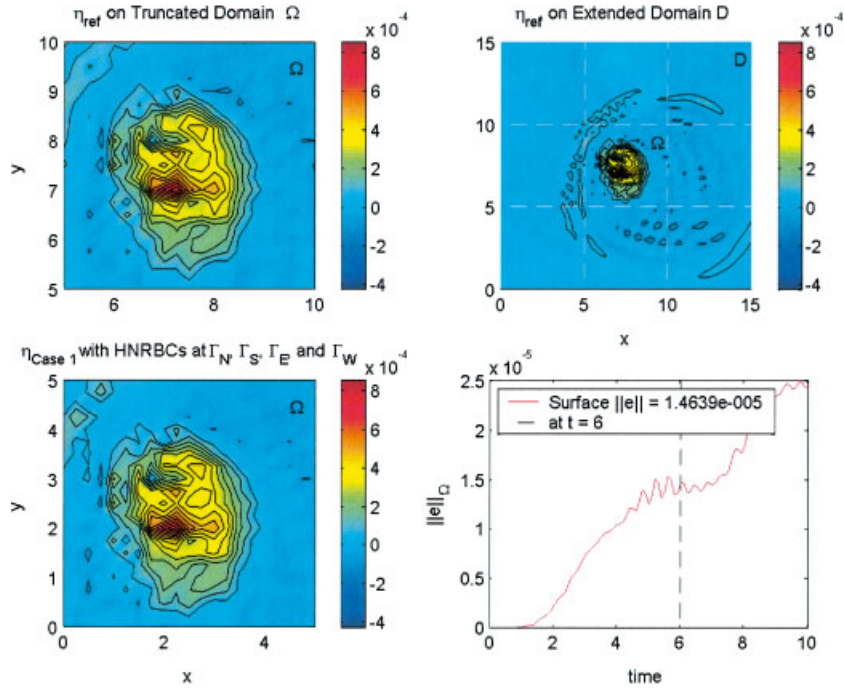*Int. J. Numer. Meth. Fluids* 2004; **46**(4)

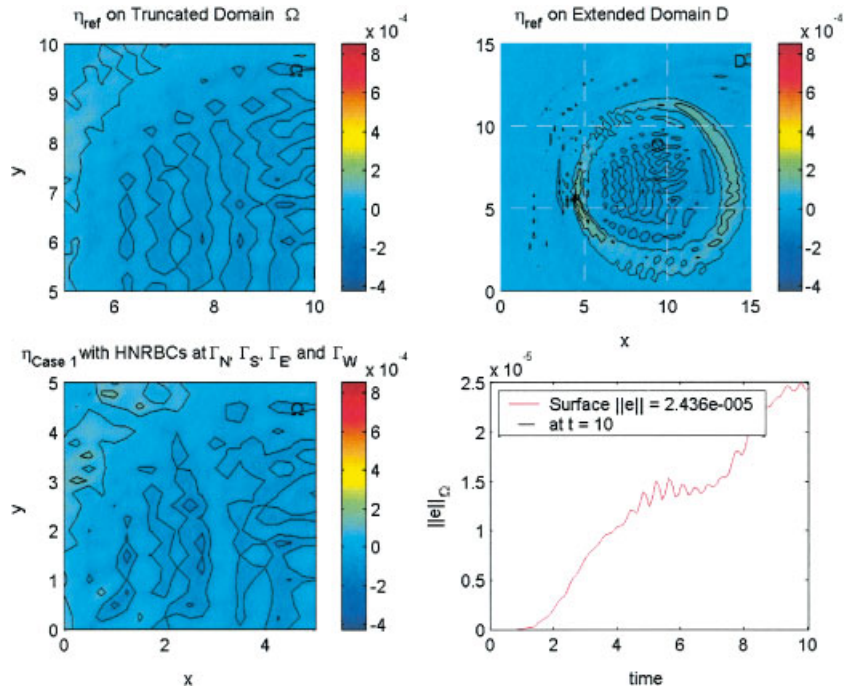Plate 6. Single layer problem, the solution at $t = 6$ after the second event has been initiated.

Plate 7. Single layer problem, the solution at $t = 10$. The spurious
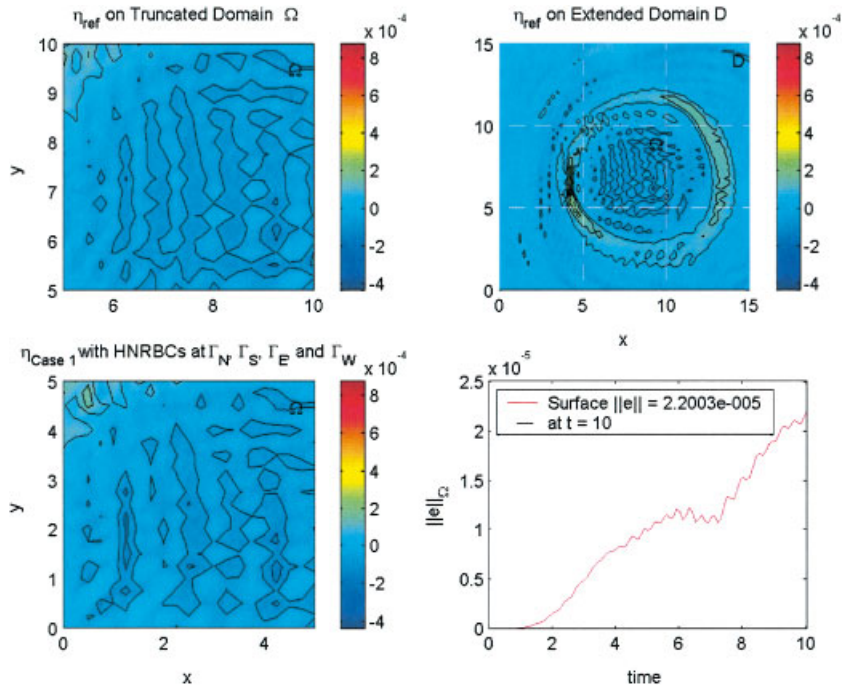reflection is evident at the bottom left plot.

Plate 8. Single layer problem, the solution at $t = 10$, with advection parameters $U = 0.4$, $V = -0.15$.
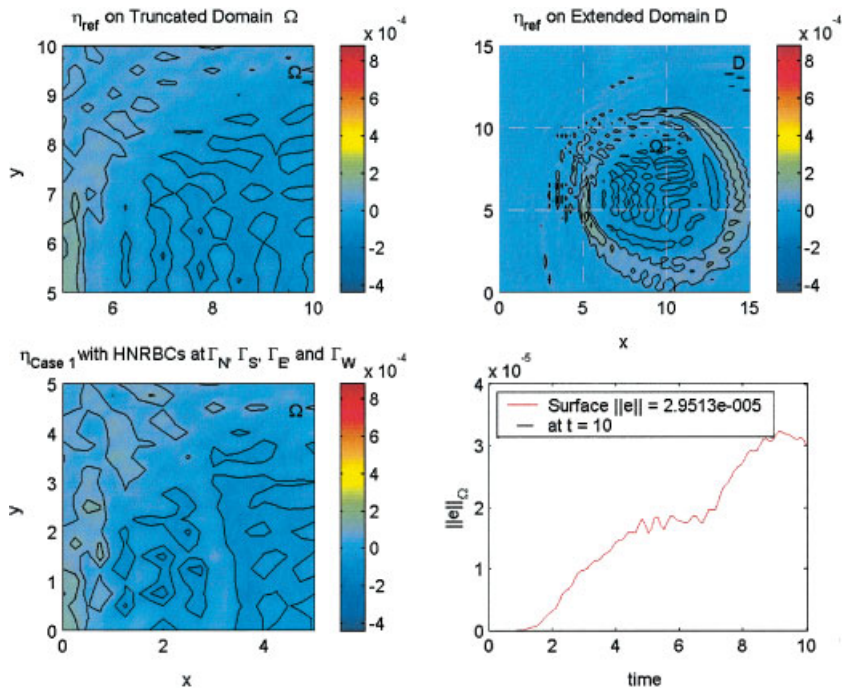

Plate 9. Single layer problem, the solution at $t = 10$, with advection parameters $U = 0.6$, $V = -0.35$.

Published in 2004 by John Wiley & Sons, Ltd.

Int. J. Numer. Meth. Fluids 2004; **46**(4)

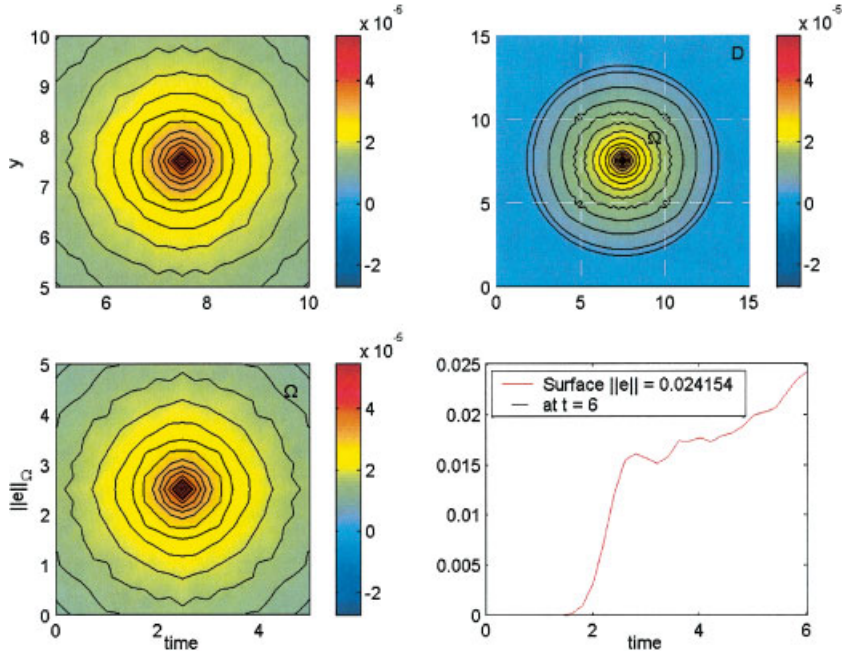Plate 10. Solution at $t = 6$ using auxiliary variable formulation with $J = 20$ and no advection.
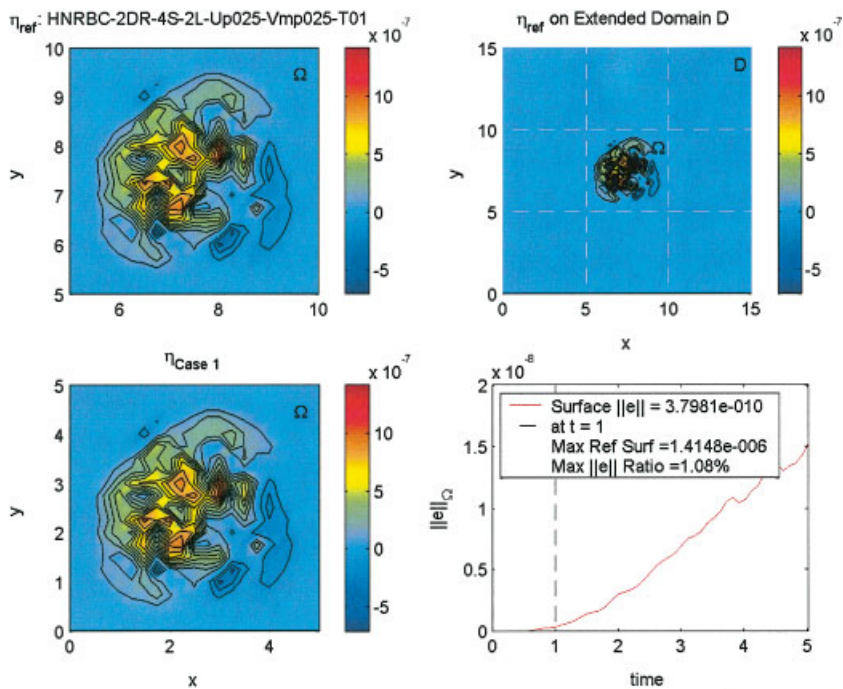
Plate 11. The two-layer problem, the solution at $t = 1$ after the initiation of disturbance.
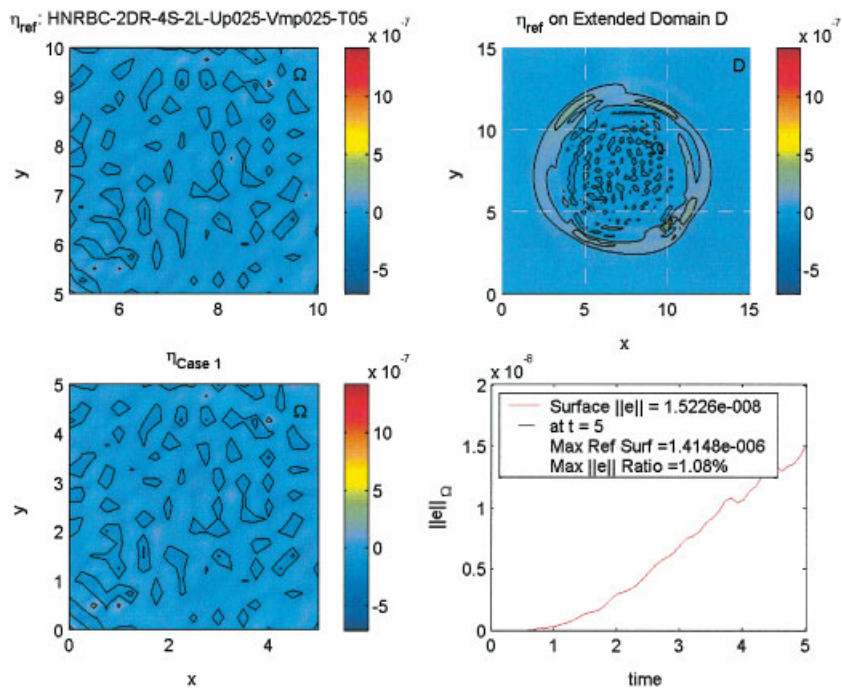
Published in 2004 by John Wiley & Sons, Ltd.

Int. J. Numer. Meth. Fluids 2004; **46**(4)

Plate 12. The two-layer problem, the solution at $t = 5$. Some noise
at boundaries of bottom left plot is evident.

In the second variation (Plate 9), the magnitude of the advection constants was increased to $U = 0.6$ and $V = -0.35$. The tendency to the southeast, as well as the error measurement, has increased.

These results indicate that the model is behaving as expected with regards to the rate and direction of advection. However, as the magnitude of the advection constants is increased, the measured error will also increase. In the current example, the magnitude of the advection is 4 to 7 times greater than the magnitude of the depth. In a real world problem, where the open ocean is the medium of propagation, advection constants are expected to be significantly smaller.

The next example involves a persistent point source which is turned on at $t = 0$ in the center of the computational domain. The computational parameters are $\Delta x = \Delta y = 0.25$, and $\Delta t = 0.1$. The parameters $C_0 = 1$ and $U = V = f = 0$ are used. The auxiliary variable formulation of the Higdon boundary conditions are applied along all four sides of the domain, with $C_j = 1$ for all the j's. Notice that since there is no advection, the auxiliary variable formulation is much simpler, see e.g. Reference [38]. The reference domain $\mathcal{D}^*$ is taken here to be large enough that during the computation time $0 \leqslant t \leqslant 6$ the wave front does not reach the extended outer boundaries at all (although it does, of course, pass the truncated boundary $\mathcal{B}$). We define the relative error measure

$$E(t) = \sqrt{\frac{\sum_{i=1}^{N_x} \sum_{j=1}^{N_y} [\eta_{\text{ref}}(x_i, y_j, t) - \eta(x_i, y_j, t)]^2}{\sum_{i=1}^{N_x} \sum_{j=1}^{N_y} \eta_{\text{ref}}^2(x_i, y_j, t)}} \qquad (40)$$

Figure 3 shows the maximum relative error during $0 \leqslant t \leqslant 6$ as a function of the Higdon order J, for $1 \leqslant J \leqslant 20$. The error reduces sharply when passing from $J = 1$ (the Sommerfeld-like condition) to $J = 2$, then oscillates slightly when J is further increased, and levels off at about 2.5%. The error cannot be reduced further without also refining the grid and choosing a smaller time-step size. With both Higdon formulations, no instability has been observed in this case. For additional examples where the error is measured for increasing J, see References [37, 40].

Plate 10 shows the comparison of the computed solution with the reference solution with $J = 20$ at $t = 6$. Very good agreement between the two solutions is observed.

5.2. A two-layer scheme incorporating advection

In this example the domains Ω and $\mathcal{D}$ as described before with identical positioning of the Higdon OBCs are utilized. The following problem parameters are used:

$$\Delta x = \Delta y = 0.25, \quad \Delta t = 0.1$$

$$g = 10, \quad f = 0.5$$

$$\Theta_i = \{0.03, 0.07\}, \quad \rho_i = \{1, 1.05\}$$

$$U_i = \{0.025, 0.025\}, \quad V_i = \{-0.025, -0.025\}$$

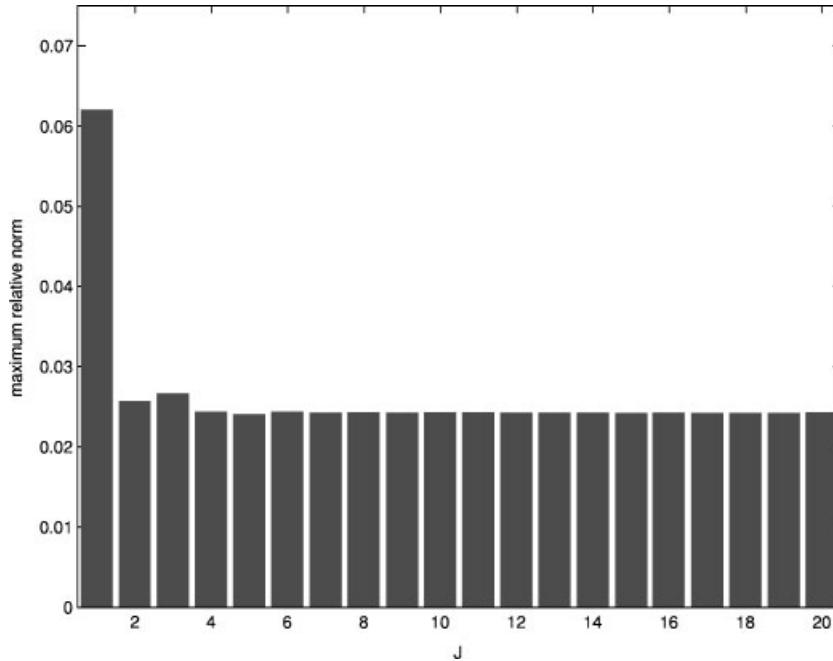$$J = 5, \quad C_j = \{0.6, 0.7, 0.8, 0.9, 1\}$$

Figure 3. Maximum relative error for $1 \leqslant J \leqslant 20$.

Correcting the C_j's for advection yields

$$C_j^{\text{east}} = \{0.625, 0.725, 0.825, 0.925, 1.025\}, \quad C_j^{\text{north}} = \{0.575, 0.675, 0.775, 0.875, 0.975\}$$

$$C_j^{\text{west}} = \{0.575, 0.675, 0.775, 0.875, 0.975\}, \quad C_j^{\text{south}} = \{0.625, 0.725, 0.825, 0.925, 1.025\}$$

A single physical disturbance is initiated in Ω and is given by

$$S_{L_1}^{t=0.1} = \begin{cases} 0.000001 \times \text{rand}(-0.5, 0.5) & \text{if } 2 \leqslant x, y \leqslant 3 \\ 0 & \text{otherwise} \end{cases} \tag{41}$$

where $S_{L_1}^{t=0.1}(x, y)$ represents a disturbance initiated in L_1 at $t = 0.1$ and $\text{rand}(-0.5, 0.5)$ is a random number on the interval $[-0.5, 0.5]$. The example is run for five time steps.

At $t = 1$ (Plate 11), the disturbance has been underway for approximately 1 s. Minimal spurious reflection occurs at the boundaries. In the lower-right plot two additional measurements are noted. The first, 'Max Ref Surf' is $|\eta|_{\max}$ measured over the entire run. The next, 'Max $\|e\|$ Ratio' is given by

$$\text{Max } \|e\| \text{Ratio} = \frac{\|e\|_{\max}}{|\eta|_{\max}} \tag{42}$$

Since both are maxima extracted from the data generated over the entire run, they will not change with time.

At $t = 5$ (Plate 12), most of the wave action has left Ω. The residual action in the truncated domains are, for the most part, similar. There is, however, some visible difference near the boundaries resultant from spurious reflection. The lower-right plot reports

$$\text{Max} \, \|e\| \text{Ratio} = 1.08\%$$

That is to say, the maximum error norm $\|e\|$ at $t = 5$ was 1.08% of the $|\eta|_{\max}$.

APPENDIX A. FORMULATION USING AUXILIARY VARIABLES

In this section, we develop the auxiliary variable formulation for the advective case. We first replace the Higdon condition

$$H_J: \quad \left[\prod_{j=1}^{J} \left(\frac{\partial}{\partial t} + C_j^+ \frac{\partial}{\partial v} \right) \right] \eta = 0 \quad \text{on } \mathscr{B} \tag{A1}$$

where

$$\begin{aligned} C_j^+ &= C_j + U, \quad j = 0, \ldots, J \\ C_j^- &= C_j - U, \quad j = 0, \ldots, J \end{aligned} \tag{A2}$$

with the equivalent condition

$$H_J: \quad \left[\prod_{j=1}^{J} \left(\frac{\partial}{\partial v} + \frac{1}{C_j^+} \frac{\partial}{\partial t} \right) \right] \eta = 0 \quad \text{on } \mathscr{B} \tag{A3}$$

Again, to fix ideas we consider Γ_E where $\partial/\partial v = \partial/\partial x$. Now, we introduce the auxiliary functions $\phi_1, \ldots, \phi_{J-1}$, which are defined on $\mathscr{B}$ as well as in the exterior domain D. Eventually, we shall use these functions only on $\mathscr{B}$, but the derivation requires that they be defined in D as well, or at least in a non-vanishing region adjacent to $\mathscr{B}$. The functions ϕ_j are defined via the relations

$$\left(\frac{\partial}{\partial x} + \frac{1}{C_1^+} \frac{\partial}{\partial t} \right) \eta = \phi_1 \tag{A4}$$

$$\left(\frac{\partial}{\partial x} + \frac{1}{C_2^+} \frac{\partial}{\partial t} \right) \phi_1 = \phi_2 \tag{A5}$$

$$\vdots$$

$$\left(\frac{\partial}{\partial x} + \frac{1}{C_J^+} \frac{\partial}{\partial t} \right) \phi_{J-1} = 0 \tag{A6}$$

By definition, these relations hold in D, and also on $\mathscr{B}$. It is easy to see that (A4)–(A6), when imposed as boundary conditions on $\mathscr{B}$, are equivalent to the single boundary condition (A3). If we also define

$$\phi_0 \equiv \eta, \quad \phi_J \equiv 0 \tag{A7}$$

then we can write (A4)–(A6) concisely as

$$\left(\frac{\partial}{\partial x} + \frac{1}{C_j^+} \frac{\partial}{\partial t} \right) \phi_{j-1} = \phi_j, \quad j = 1, \ldots, J \tag{A8}$$

This set of conditions involves only first-order derivatives. However, due to the appearance of the x-derivative in (A8), one cannot discretize the ϕ_j on the boundary alone. Therefore we shall manipulate (A8) in order to get rid of the x-derivative.

The function η satisfies the wave equation (5) in D. The function ϕ_1 is obtained by applying a linear constant coefficient operator to η, as in (A4); hence it is clear that ϕ_1 also satisfies the same equation in D. Similarly, we deduce that each of the functions ϕ_j satisfies a wave equation like (5), namely,

$$C_0^2 \frac{\partial^2 \phi_{j-1}}{\partial x^2} + C_0^2 \frac{\partial^2 \phi_{j-1}}{\partial y^2} - \frac{\mathrm{D}^2 \phi_{j-1}}{\mathrm{D}t^2} - f^2 \phi_{j-1} = 0 \tag{A9}$$

Here, we need the assumption that C_0 and f do not depend on x or on t. Let us factor $C_0^2(\partial^2 \phi_{j-1}/\partial x^2) - \mathrm{D}^2 \phi_{j-1}/\mathrm{D}t^2$ and use the definition of the operator $\mathrm{D}/\mathrm{D}t$

$$
\begin{aligned}
C_0^2 \frac{\partial^2}{\partial x^2} \phi_{j-1} - \frac{\mathrm{D}^2 \phi_{j-1}}{\mathrm{D}t^2} &= \left(C_0 \frac{\partial}{\partial x} - \frac{\mathrm{D}}{\mathrm{D}t} \right) \left(C_0 \frac{\partial}{\partial x} + \frac{\mathrm{D}}{\mathrm{D}t} \right) \phi_{j-1} \\
&= \left(C_0^- \frac{\partial}{\partial x} - \frac{\partial}{\partial t} - V \frac{\partial}{\partial y} \right) \left(C_0^+ \frac{\partial}{\partial x} + \frac{\partial}{\partial t} + V \frac{\partial}{\partial y} \right) \phi_{j-1}
\end{aligned}
\tag{A10}
$$

Using the auxiliary variables we have

$$
\begin{aligned}
\left(C_0^+ \frac{\partial}{\partial x} + \frac{\partial}{\partial t} + V \frac{\partial}{\partial y} \right) \phi_{j-1} &= C_0^+ \left(\frac{\partial}{\partial x} + \frac{1}{C_0^+} \frac{\partial}{\partial t} + \frac{V}{C_0^+} \frac{\partial}{\partial y} \right) \phi_{j-1} \\
&= C_0^+ \left(\phi_j - \frac{1}{C_j^+} \frac{\partial}{\partial t} \phi_{j-1} + \frac{1}{C_0^+} \frac{\partial}{\partial t} \phi_{j-1} + \frac{V}{C_0^+} \frac{\partial}{\partial y} \phi_{j-1} \right) \\
&= C_0^+ \left(\phi_j + \left(\left(\frac{1}{C_0^+} - \frac{1}{C_j^+} \right) \frac{\partial}{\partial t} + \frac{V}{C_0^+} \frac{\partial}{\partial y} \right) \phi_{j-1} \right)
\end{aligned}
\tag{A11}
$$

Now we have to operate on this with $C_0^-(\partial/\partial x) - (\partial/\partial t) - V\partial/\partial y$ and add the remaining 2 terms of (A9)

$$
C_0^+ C_0^- \left(\frac{\partial}{\partial x} - \frac{1}{C_0^-} \frac{\partial}{\partial t} - \frac{V}{C_0^-} \frac{\partial}{\partial y} \right) \left(\phi_j + \left(\left(\frac{1}{C_0^+} - \frac{1}{C_j^+} \right) \frac{\partial}{\partial t} + \frac{V}{C_0^+} \frac{\partial}{\partial y} \right) \phi_{j-1} \right)
$$

$$+C_0^2 \frac{\partial^2}{\partial y^2} \phi_{j-1} - f^2 \phi_{j-1}$$

$$= C_0^+ C_0^- \left\{ \phi_{j+1} - \frac{1}{C_{j+1}^+} \frac{\partial}{\partial t} \phi_j - \frac{1}{C_0^-} \frac{\partial}{\partial t} \phi_j - \frac{V}{C_0^-} \frac{\partial}{\partial y} \phi_j \right.$$

$$+ \left(\frac{1}{C_0^+} - \frac{1}{C_j^+} \right) \frac{\partial}{\partial t} \left(\phi_j - \frac{1}{C_j^+} \frac{\partial}{\partial t} \phi_{j-1} \right)$$

$$- \frac{1}{C_0^-} \left(\frac{1}{C_0^+} - \frac{1}{C_j^+} \right) \frac{\partial^2}{\partial t^2} \phi_{j-1} - \frac{V}{C_0^-} \left(\frac{1}{C_0^+} - \frac{1}{C_j^+} \right) \frac{\partial^2}{\partial y \partial t} \phi_{j-1}$$

$$+ \frac{V}{C_0^+} \frac{\partial}{\partial y} \left(\phi_j - \frac{1}{C_j^+} \frac{\partial}{\partial t} \phi_{j-1} \right) - \frac{V}{C_0^- C_0^+} \frac{\partial^2}{\partial y \partial t} \phi_{j-1} - \frac{V^2}{C_0^- C_0^+} \frac{\partial^2}{\partial y^2} \phi_{j-1}$$

$$\left. + \frac{C_0^2}{C_0^- C_0^+} \frac{\partial^2}{\partial y^2} \phi_{j-1} - \frac{f^2}{C_0^- C_0^+} \phi_{j-1} \right\} = 0 \tag{A12}$$

Now we collect terms

$$\phi_{j-1} + \left(\frac{1}{C_0^+} - \frac{1}{C_j^+} - \frac{1}{C_{j+1}^+} - \frac{1}{C_0^-} \right) \frac{\partial}{\partial t} \phi_j + V \left(\frac{1}{C_0^+} - \frac{1}{C_0^-} \right) \frac{\partial}{\partial y} \phi_j$$

$$- \left(\frac{1}{C_0^+} - \frac{1}{C_j^+} \right) \left(\frac{1}{C_j^+} + \frac{1}{C_0^-} \right) \frac{\partial^2}{\partial t^2} \phi_{j-1} - \left[\frac{V}{C_0^-} \left(\frac{2}{C_0^+} - \frac{1}{C_j^+} \right) + \frac{V}{C_0^+ C_j^+} \right] \frac{\partial^2}{\partial y \partial t} \phi_{j-1}$$

$$+ \frac{C_0^2 - V^2}{C_0^+ C_0^-} \frac{\partial^2}{\partial y^2} \phi_{j-1} - \frac{f^2}{C_0^+ C_0^-} \phi_{j-1} = 0 \tag{A13}$$

Add to this

$$\phi_0 = \eta \tag{A14}$$

$$\left(\partial_x + \frac{1}{C_1^+} \partial_t \right) \eta = \phi_1 \tag{A15}$$

Eqs. (A13)–(A15) constitute a high-order boundary condition which involves only first and second time derivatives and tangential derivatives along the boundary. It can be discretized and combined with the interior finite difference scheme in a way similar to that used in Reference [38] for the simpler case of zero mean flow.

REFERENCES

 1. Givoli D. *Numerical Methods for Problems in Infinite Domains.* Elsevier: Amsterdam, 1992.
 2. Engquist B, Majda A. Absorbing boundary conditions for the numerical simulation of waves. *Mathematics of Computation* 1977; **31**(139):629–651.
 3. Engquist B, Majda A. Radiation boundary conditions for acoustic and elastic wave calculations. *Communications on Pure and Applied Mathematics* 1979; **32**:313–357.
 4. Perkey DJ, Kreitzberg CW. A time-dependent lateral boundary scheme for limited-area primitive equation models. *Monthly Weather Review* 1976; **104**:744–755.
 5. Davies HC. A lateral boundary formulation for multi-level prediction models. *Quarterly Journal of Royal Meteorological Society* 1976; **102**:405–418.
 6. Israeli H, Orszag SA. Approximation of radiation boundary conditions. *Journal of Computational Physics* 1981; **41**:115–135.
 7. Hodur RM. The Naval Research Laboratory's coupled ocean/atmosphere mesoscale prediction system (COAMPS). *Monthly Weather Review* 1997; **125**:1414–1430.
 8. Berenger J-P. A perfectly matched layer for the absorption of electromagnetic waves. *Journal of Computational Physics* 1994; **127**:185–200.
 9. Clement A. Coupling of two absorbing boundary condition for 2D time-domain simulation of free surface gravity waves. *Journal of Computational Physics* 1996; **126**:139–159.
10. Karni S. Far field filtering operators for suppression of reflections from artificial boundaries. *SIAM Journal on Numerical Analysis* 1996; **33**:1014–1047.
11. Kosloff R, Kosloff D. Absorbing boundaries for wave propagation problems. *Journal of Computational Physics* 1986; **63**:363–376.
12. Hu FQ. On absorbing boundary conditions for linearized Euler equations by a perfectly matched layer. *Journal of Computational Physics* 1996; **129**:201–216.
13. Collino F. Perfectly matched absorbing layers for paralaxial equations. *Journal of Computational Physics* 1996; **131**:164–180.
14. Hayder ME, Atkins HL. Experience with PML boundary conditions in fluid flow computation. In *Collection of Abstract of Symposium on Computational Methods for Unbounded Domains*, Gears TL (ed.). University of Colorado, Boulder. Kluwer Academic Press: Dordrecht, July 27–31, 1997.
15. Hayder HE, Hu FQ, Hussaini MY. Towards perfectly absorbing boundary conditions for Euler equations. *AIAA Journal* 1999; **37**(8):912–918.
16. Darblade G, Baraille R, le Roux A-Y, Carton X, Pinchon D. Conditions limites non reflechissantes pour un mod'ele de Saint-Venant bidimensionnel barotrope linearise. *Comptes Rendus de L Academic des Sciences, Paris* 1997; **324**:485–490.
17. Navon IM, Neta B, Hussaini MY. A perfectly matched layer approach to the linearized shallow water equations model. *Monthly Weather Review* 2004; **132**:1369–1378.
18. Tsynkov SV. Numerical solution of problems on unbounded domains. A Review. *Applied Numerical Mathematics* 1998; **27**:465–532.
19. Givoli D. Exact representations on artificial interfaces and applications in mechanics. *Applied Mechanical Review* 1999; **52**:333–349.
20. Hagstrom T. Radiation boundary conditions for the numerical simulation of waves. *Acta Numerica* 1999; **8**: 47–106.
21. Bayliss A, Turkel E. Radiation boundary conditions for wave-like equations. *Communication on Pure and Applied Mathematics* 1980; **33**:707–725.
22. Keller JB, Givoli D. Exact non-reflecting boundary conditions. *Journal of Computational Physics* 1989; **82**: 172–192.
23. Givoli D, Keller JB. Non-reflecting boundary conditions for elastic waves. *Wave Motion* 1990; **12**:261–279.
24. Collino F. High order absorbing boundary conditions for wave propagation models. Straight line boundary and corner cases. In *Proceedings of 2nd International Conference on Mathematical & Numerical Aspects of Wave Propagation*, Kleinman R *et al.* (eds.), SIAM: Delaware, 1993; 161–171.
25. Grote MJ, Keller JB. Nonreflecting boundary conditions for time dependent scattering. *Journal of Computational Physics* 1996; **127**:52–65.
26. Grote MJ, Keller JB. Nonreflecting boundary conditions for elastic waves. *SIAM Journal on Applied Mathematics* 2000; **60**:803–819.
27. Sofronov IL. Conditions for complete transparency on the sphere for the three-dimensional wave equation. *Russian Academy of Sciences Doklady Mathematics* 1993; **46**:397–401.
28. Hagstrom T, Hariharan SI. A formulation of asymptotic and exact boundary conditions using local operators. *Applied Numerical Mathematics* 1998; **27**:403–416.
29. Guddati MN, Tassoulas JL. Continued-fraction absorbing boundary conditions for the wave equation. *Journal of Computational Acoustics* 2000; **8**:139–156.

30. Givoli D. High-order non-reflecting boundary conditions without high-order derivatives. *Journal of Computational Physics* 2001; **170**:849–870.
31. Higdon RL. Absorbing boundary conditions for difference approximations to the multi-dimensional wave equation. *Mathematics of Computation* 1986; **47**:437–459.
32. Higdon RL. Numerical absorbing boundary conditions for the wave equation. *Mathematics of Computation* 1987; **49**:65–90.
33. Higdon RL. Radiation boundary conditions for elastic wave propagation. *SIAM Journal on Numerical Analysis* 1990; **27**:831–870.
34. Higdon RL. Absorbing boundary conditions for elastic waves. *Geophysics* 1991; **56**:231–241.
35. Higdon RL. Radiation boundary conditions for dispersive waves. *SIAM Journal on Numerical Analysis* 1994; **31**:64–100.
36. Givoli D, Neta B. High-order Higdon non-reflecting boundary conditions for the shallow water equations. NPS-MA-02-001, *Technical Report*. Naval Postgraduate School, Monterey, CA, 2002.
37. Givoli D, Neta B. High-order non-reflecting boundary conditions for dispersive waves. *Wave Motion* 2003; **37**:257–271.
38. Givoli D, Neta B. High-order non-reflecting boundary scheme for time-dependent waves. *Journal of Computational Physics* 2003; **186**:24–46.
39. Pedlosky J. *Geophysical Fluid Dynamics*. Springer: New York, 1987.
40. van Joolen VJ. Application of Higdon Non-Reflecting Boundary Conditions to Shallow Water Models. *Ph.D. Thesis*, Naval Postgraduate School, Monterey, CA, 2003.
41. Cushman-Roisin B. *Introduction to Geophysical Fluid Dynamics*. Prentice-Hall: Englewood Cliffs, NJ, 1994.
42. Higdon RL. Absorbing boundary conditions for acoustic and elastic waves in stratified media. *Journal of Computational Physics* 1992; **101**:386–418.